INVESTIGATION ON ASH FOULING FORMATION OF INDUCED FAN BLADE AND HEAT EXCHANGER SURFACE IN A 1000 MW COAL-FIRED POWER PLANT

by

He-Xin LIU, Jia-Fan XIAO, Hou-Zhang TAN*, Yi-Bin WANG, and Fu-Xin YANG

MOE Key Laboratory of Thermo-Fluid Science and Engineering,
Xi'an Jiaotong University, Xi'an, Shannxi, China

Original scientific paper
https://doi.org/10.2298/TSCI200311269L

The control of fouling deposition on the main equipment has always been an important issue concerned by scientific research and industrial application. However, severe fouling deposits on the induced fan blade and the low temperature economiser were found in a 1000 MW coal-fired power plant with ultra-low emission. The deposit samples were collected and analysed through X-ray diffraction spectrometer, X-ray fluorescence, elemental analyser and SEM with energy dispersive spectrometers. The result shows that the deposits are mainly composed of tschermigite $(NH_4)Al(SO_4)_2 \cdot 12H_2O$, letovicite $(NH_4)_3H(SO_4)_2$, calcium sulphate $CaSO_4$, and quartz SiO_2. The ammonium sulphate is the main component of the fouling deposits. It acts as an adhesive and makes an important contribution to the deposition. The analysis shows that the ammonia slip from denitrification system and the unreasonable temperature setting are the main reasons for fouling deposition. It is suggested that the high concentration of ammonium slip at denitrification system and the rapid condensation of the sulphuric acid mist at heat exchanger should be paid more attention in coal-fired power plants.

Key words: *fouling deposition, ammonium sulphate, coal-fired power plant, induced fan blade, low temperature economiser*

Introduction

With the improvement of ecological environment awareness, the impacts of pollutant emission from coal-fired power plants on frequent haze weather have gradually attracted attention [1, 2]. Currently, China has fully carried out strict ultra-low emission standard for coal-fired power plants, which specifies particulate matter (PM), sulphur dioxide (SO_2), and NO_x shall not exceed 5, 35, and 50 mg/Nm^3 [3]. Correspondingly, the technologies that achieve the ultra-low emission target through a series of processes or devices are called ultra-low emission technologies. In terms of PM removal, there are many ways such as the low-low temperature electrostatic precipitator (LLT-ESP) [4], wet

*Corresponding author, e-mail: hzt@mail.xjtu.edu.cn

electrostatic precipitator (WESP) [5], and high-frequency power supply [6]. For the control of SO_2, the more effective technologies include the single tower integrated desulphurization and dust removal purification (SPC-3D) [7], double absorption tower and two circulations per tower [8]. Besides, the main emission reduction technologies for NO_x consist of low NO_x combustion [9], selective catalytic reduction (SCR) and selective non-catalytic reduction (SNCR) [10].

Although the ultra-low emission technologies are effective ways to control the main air pollutants, there are still many new problems existing in coal-fired units during technical reconstruction. For example, the gaseous reductants, ammonia or urea solution, which are injected in SCR, react chemically with the NO_x in the catalyst layers, but the vanadium-containing catalyst can convert about 1% of SO_2 into SO_3 in this process [11]. Then, some of the gaseous reductants will directly pass through the SCR system and react with sulphuric acid downstream to produce ammonium sulphate or bisulphate (ABS) [12]. Compared with ammonium sulphate that exists as dry solid powders within the operating temperature range of the downstream air preheater, ABS presents sticky and easily induces serious acidic deposit on the metal elements of the air preheater. Menasha *et al*. [13] showed that the formation temperature of ABS is 227-247 °C for the typical flue gas with ammonia of 2-10 ppm and sulphuric acid of 5-45 ppm. Chothani [14] observed that ammonium sulphate becomes the main component in the flue gas when the molar ratio of ammonia to SO_3 is greater than 2. It can be summarized that the formation of ABS in the flue gas is affected by three main factors: consisting of temperature, concentration, and molar ratio of ammonia to SO_3. Furthermore, the concentration product of ammonia and sulphur trioxide can also reflect the formation rate of ABS, which means the low ammonia slip can also easily form ABS deposits when the concentration of SO_3 is high enough. Thus, high conversion rate of SO_2 to SO_3 and ammonia slip from SCR are one of important causes of serious blockage of ABS. In addition, in order to remove PM and sulphur more efficiently, LLT-ESP technology has been widely used in the Chinese power plants with ultra-low emission modification, which maintains the flue gas temperature of about 85-95 °C before ESP through a heat exchanger [15]. The SO_3 in the flue gas can react with water vapour to form the sulphuric acid mist. These mist then stick to the surface of PM and improve the removal and collection of SO_3 by ESP [16]. Although the sulphuric acid mist can be removed under design conditions, it may fail under actual conditions and then severe corrosion and deposition will occur at the downstream of the LLT-ESP because of low temperature. Therefore, in order to address the problems in the ultra-low emission modification, it is of scientific and practical significance to conduct study on the ash fouling formation of coal-fired unit equipment to provide more reasonable suggestions.

In this work, serious fouling deposits were investigated on the blade of the induced draft fan and the surface of the two-stage low temperature economiser (LTE) in a 1000 MW coal-fired power plant. The deposition and fouling were firstly sampled when the coal-fired unit was shut down. The chemical compositions and micro-morphologies of these samples were characterized through X-ray diffraction (XRD), X-ray fluorescence (XRF), and SAM with energy dispersive spectrometers (SEM-EDS). Then the performance of upstream equipment and the formation of the fouling were then analysed and evaluated. Finally, based on the aforementioned analysis, a formation mechanism of ash fouling was proposed for further understanding ash fouling problems in coal-fired power plants.

Field parameters and sampling location

The essential information of the coal-fired power plants will be presented, including system composition, operating temperature, coal properties, and ash compositions. Then, the thermodynamic model of the acid dew point for coal-fired flue gas will be provided, which can be used to evaluate the change of the acid dew point temperature with coal properties and further analyse the formation mechanism of fouling deposition.

Coal-fired power plant

The research object was the No. 1 unit of a 1000 MW ultra-supercritical coal-fired power plant with ultra-low emission, which was located in Shouguang City, Shandong Province. As shown in fig. 1, a three-layer SCR with V_2O_5-TiO_2 catalyst was equipped and the design efficiency of denitration reached 87%. The first two layers of the catalyst were enable while the last one was on standby. A two-stage LTE was used for recovering latent heat of the flue gas and improving the removal efficiency of ESP and WESP. The first stage LTE was installed at the inlet of the ESP and the second LTE was located at the inlet of the WFGD. The induced draft fan was installed at the outlet of the ESP to supply the driving force for flue gas-flow and balance the system resistance. The removal efficiency of PM for the ESP was higher than 99%. The distributed control system (DCS) showed that the concentration of PM at the outlet of ESP was about 5 mg/m^3 with small fluctuations, and the concentration of SO_2 was about 1200 mg/m^3 at full load.

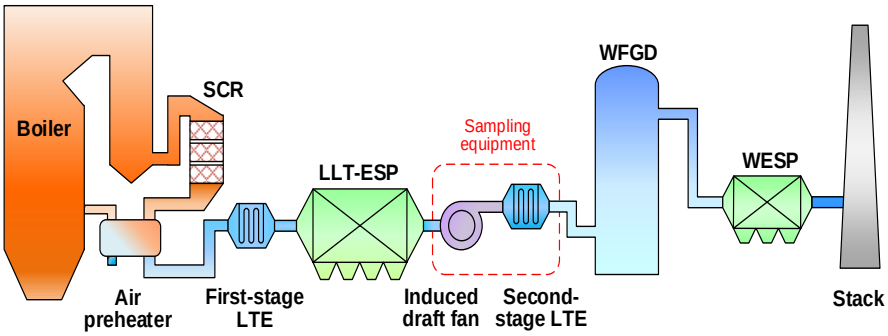

Figure 1. Schematic diagrams of the coal-fired power plant and the sampling equipment

According to the data of DCS, the boiler load was distributed between 50-100%. When the boiler was at full capacity, the flue gas temperature of the outlet for the first-stage LTE and the second-stage LTE was ranged within 103-121 °C and 98-101 °C, respectively. While the boiler was at 50% capacity, the temperature ranges were 100-111 °C and 95-100 °C for the first-stage and the second-stage LTE, respectively. Meanwhile, it could be found that the temperature drop of the second-stage LTE would experience 15-20 °C when the temperature of the first-stage LTE decreased 2-5 °C.

Coal properties and ash compositions

The typical properties and the ash compositions of the coal are presented in tabs. 1 and 2. It can be seen that the sulphur contents in design coal and checked coal are both below than 1%, but severe fouling deposits are found at the downstream equipment of ESP, which indicates that ammonia escape in SCR systems may have been existing.

Table 1. Typical properties of design coal and checked coal

Samples	Proximate analysis [%]				Element analysis [%]					*LHV* [MJkg^{-1}]
	M_t	M_{ad}	A_{ar}	V_{daf}	C_{ar}	H_{ar}	O_{ar}	N_{ar}	St_{ar}	$Q_{ar,net}$
Design coal	18.50	10.66	10.24	35.61	57.33	3.26	9.34	0.61	0.63	21.23
Checked coal	17.90	9.33	15.10	34.68	53.25	3.00	9.70	0.58	0.47	20.02

Note: The subscripts t and ad represent the total and the air dried basis, respectively;
the subscript ar and daf represent the air received basis and the dry ash-free basis, respectively

Table 2. Ash compositions of design coal and checked coal [wt.%]

Samples	Fe_2O_3	Al_2O_3	CaO	MgO	SiO_2	TiO_2	SO_3	K_2O	Na_2O
Design coal	11.52	18.38	12.75	1.60	46.12	0.81	6.33	1.31	0.66
Checked coal	8.81	18.87	8.3	1.51	56.06	1.04	2.75	1.36	0.74

Flue gas acid dew point

According to the coal properties and ash compositions, the acid dew point of the flue gas can be estimated using thermodynamic method, which is given:

$$t_1 = t_s + \frac{\beta^3 \sqrt{S_{ar,zs}}}{1.05^{\alpha_{fh}} A_{ar,zs}} \tag{1}$$

$$S_{ar,zs} = 1000 \frac{S_{ar}}{Q_{net}} \tag{2}$$

$$A_{ar,zs} = 1000 \frac{A_{ar}}{Q_{net}} \tag{3}$$

where t_1 is the acid dew point, t_s – the water dew point, β – the parameter related to excess air coefficient and is generally set to 1.25, and $S_{ar,zs}$ and $A_{ar,zs}$ – the corrected sulphur content and the corrected ash content, respectively. The influence of fly ash content on acid dew point is corrected by α_{fh}, which can be set in the range of 0.8-0.9.

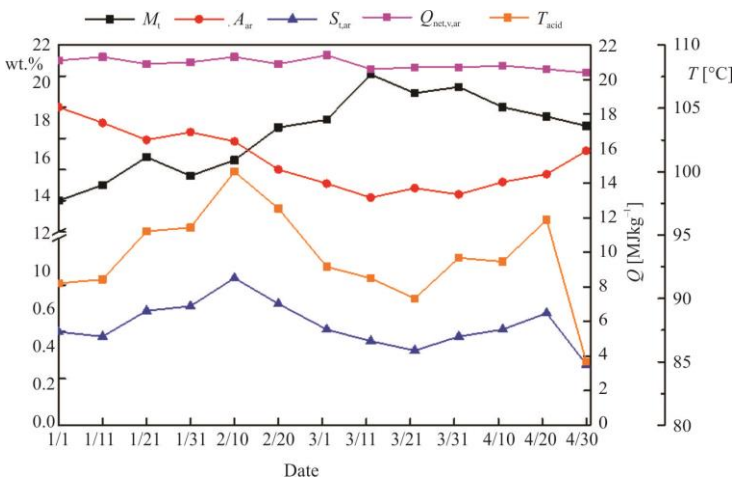

Figure 2. The coal properties from January 1st to May 1st

The coal properties and the acid dew points in the past six months are shown in fig. 2. The calculation result shows that the authentic acid dew points were between 85-100 °C. The result was lower than the inlet temperature of the LLT-ESP, which indicated that the LLT-ESP was not working under optimum conditions.

Ash sampling and analytical methods

During the 10-month operation period, the pollutant emissions of the boiler unit were lower than the ultra-low emission limits. However, when it performing scheduling outages, severe ash deposits and fouling were found on the surfaces of the induced draft fan blades and the second-stage LTE tube walls. The surfaces of the fan blade were covered uniformly by rigid fouling. The inlet of the second-stage LTE was blocked seriously by hard deposits while the outlet of the heat exchanger was crumbly deposits and dust. In order to further analyse the formation mechanism of the fouling, some ash deposits were sampled from the three locations. The sampling equipment is shown in fig. 1, and the actual situation of the fouling deposits is shown in figs. 3 and 4. The samples from the induced fan blade, the inlet of the second-stage LTE and the outlet of the second-stage LTE are named sample 1, 2, and 3 in this paper, respectively.

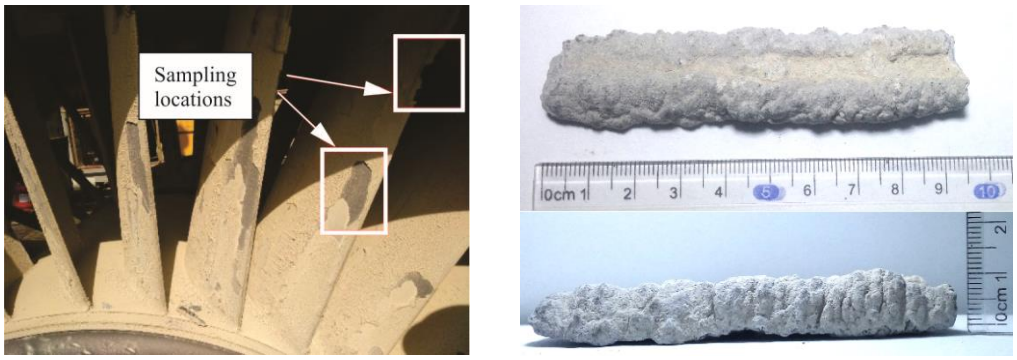

Figure 3. Fouling deposits (left) and ash morphology (right) on the fan blade

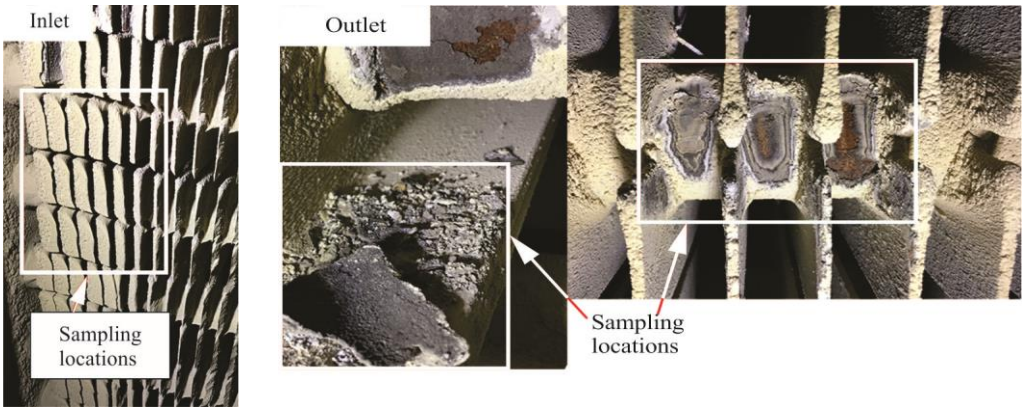

Figure 4. Fouling deposits on the inlet (left) and outlet (right) of the second-stage LTE

The collected samples were first ground in an agate mortar for 30 minutes and passed through a 200-mesh sieve to obtain fine powder samples with uniform particle sizes. These fine powder samples were then characterized and analysed by XRD (model Bruker D8

ADVANCE), XRF (model Bruker S8 Tiger), and SEM–EDS (model HITACHI SU3500). The main elements consisting of C, H, N, and S in the fine powder samples were measured through the elemental analyser (model Germany vaeeio MACRO cube), while the remaining elements in the samples were analysed through XRF. The XRD with the MDI jade6.5 software was used to identify the crystal phase composition in the samples. Furthermore, the micromorphologies of the samples were observed through the SEM-EDS.

Results and discussion

In the following passage, the elemental contents of the fouling deposits were first analysed, and then the reactions of the mineral compositions were studied. Additionally, the micromorphologies were further observed and identified. Finally, based on the above results, the formation mechanisms of the fouling deposits on the induced fan blade and heat exchanger surface were concluded and illustrated.

Elemental analysis and migration

The elemental distributions of the three samples are shown in tab. 3, and the changes of these elements are illustrated in fig. 5.

Table 3. Elemental distributions of the three fouling deposit samples

Elements [wt.%]	Sample 1 (induced fan blade)	Sample 2 (inlet of LTE)	Sample 3 (outlet of LTE)
O	51.4	51.2	47.7
S	16.5	10.0	7.9
N	5.0	4.1	2.7
H	4.0	3.3	2.1
Si	8.7	12.5	14.5
Al	6.2	8.3	8.9
Ca	2.9	4.0	4.2
Fe	2.3	3.2	6.7
K	0.5	0.9	1.2
Others	2.5	2.5	4.1

It can be seen that the total percentage of the three elements, N, O, and S, for the three samples, are 72.9%, 65.3%, and 58.3%, respectively. The high percentages indicate that ammonium sulphate minerals are rich in the three samples, and the downward trend also show that the ammonium sulphate minerals are the most serious in the induced fan blade along the flue gas-flow. According to figs. 3 and 4, the actual situations of fouling deposits also correspond to this change. In addition, tabs. 1 and 2 show that there is less sulphur in the coal and in the ash. Therefore, it can be speculated that the ammonia slip from SCR, especially in local high concentrations, can cause enrichment of sulphur by homogeneous or heterogeneous chemical reactions.

As shown in fig. 5, the mass percentages of O, S, N, and H decrease with the flow of the flue gas, and the elements in the induced fan blade are the highest. At the downstream of the LLT-ESP, the flue gas temperature was fluctuated around the acid dew point of 98 °C. Under the situation of low temperature and low particle concentration, it's easier for the coal-fired unit using SCR system to generate ammonium sulphate minerals by chemical reactions. Therefore, it can be identified that the ammonium sulphate mineral are deposited on the surface of the induced fan blade, and it may explain why the fouling deposits on the blade are

harder than that in the second-stage LTE. Furthermore, it can be seen that the mass percentages of Si, Al, Ca, and K are increasing along the direction of flue gas-flow. As non-volatile elements, these elements are mainly concentrated in the ash particles after coal burning in the boiler. As a whole, their relative contents remain essentially unchanged in the flue gas. Thus, the increase of the four elements can be attributed to the decrease in O, S, N, and H. In addition, the mass percentages of Fe in the second-stage LTE are higher than that in the induced fan blade, whose reason is mainly the different degree of corrosion as shown in figs. 3 and 4.

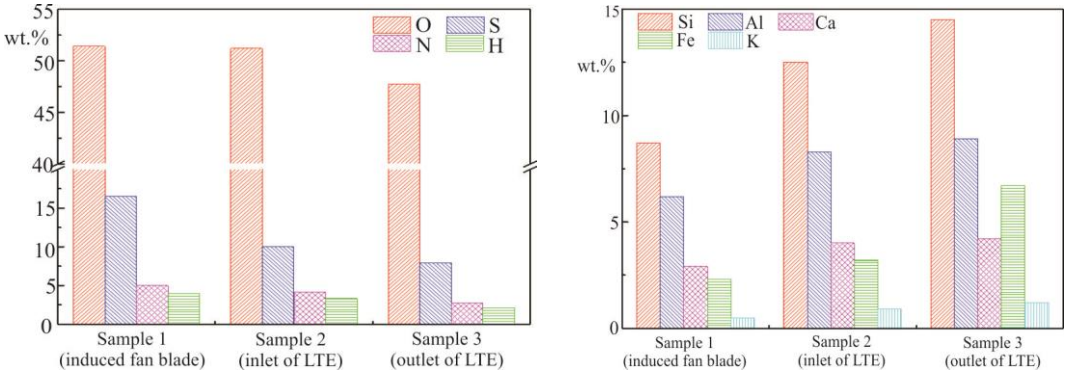

Figure 5. Mass percentages of the main elements in the three fouling deposit samples

Mineral composition and reaction

Some significant differences were observed in the crystalline phase composition between the ash samples of the induced fan blade and those of the second-stage LTE through XRD, as illustrated in fig. 6. The main crystalline phases in the sample of the induced fan blade included tschermigite $(NH_4)Al(SO_4)_2 \cdot 12H_2O$, godovikovite $(NH_4)Al(SO_4)_2$, letovicite $(NH_4)H(SO_4)_2$, calcium sulphate $CaSO_4$, calcium sulphate dehydrate $CaSO_4 \cdot 2H_2O$, and quartz SiO_2. While the samples from the second-stage LTE included tschermigite $(NH_4)Al(SO_4)_2 \cdot 12H_2O$, ferric sulphate $Fe_2(SO_4)_3$, calcium sulphate $CaSO_4$, and quartz SiO_2. It can be seen that the tschermigite exists in all of the three samples. Tschermigite is a mineral form of ammonium alum and water soluble, whose melting point is about 93.5 °C. In industrial application, ammonium sulphate is added to the concentrated solution of aluminium sulphate, and the ammonium alum will be prepared after dissolve, filtering, concentrating, cooling and separating crystal. In addition, ammonium sulphate and alumina can also react chemically to produce ammonium alum directly at high temperature [17]. According to the aforementioned properties of the ammonium sulphate mineral, it can be speculated that the tschermigite found in the ash samples can be from SCR and down-stram LLT-ESP. Meanwhile, the temperature of the flue gas may be lower than the acid dew point due to fluctuation or local heterogeneity. Therefore, the sulphuric acid mist condensed in the flue gas might react with the alumina in the ash particles to produce aluminium sulphate which is hygroscopic. Meanwhile, the ammonium escaped from SCR is also easier to react with the sulphuric acid mist and form ammonium sulphate. Finally, the tschermigite and the godovikovite are produced through the action among aluminium sulphate, ammonium sulphate and water. Moreover, high temperature can accelerate the reactions between ammonium sulphate and alumina, and the related chemical equations are listed as followed:

$$2NH_3 + SO_3 + H_2O \rightarrow (NH_4)_2 SO_4 \tag{1}$$

$$NH_3 + SO_3 + H_2O \rightarrow NH_4HSO_4 \tag{2}$$

$$4(NH_4)_2SO_4 + Al_2O_3 \rightarrow 2(NH_4)Al(SO_4)_2 + 6NH_3 + 3H_2O \tag{2}$$

$$(NH_4)_2SO_4 + Al_2(SO_4)_3 + 12H_2O \rightarrow 2(NH_4)Al(SO_4)_2 \cdot 12H_2O \tag{3}$$

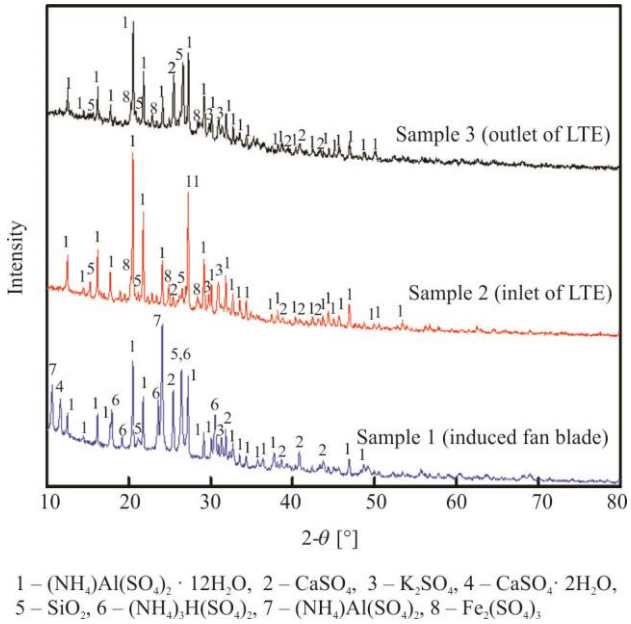

Figure 6. The XRD patterns of the three fouling deposite samples

Furthermore, the letovicite presented in the ash samples is an ammonia sulphate mineral. A study on the simultaneous measurement of gaseous ammonia and particulate ammonium found that the letovicite will be generated when the molar ratio of the ammonia and sulphuric acid is approximately equal to 1.5 [18]. The peaks of letovicite observed in the ash sample of the induced fan blade show that the stoichiometry of the ammonia and sulphuric acid is close to 1.5, and $(NH_4)_3H(SO_4)_2$ is the main product. In addition, the XRD patterns show that calcium sulphate is also one of the main components for the ash samples, which can be attributed to the high proportion of calcium oxide in the coal as shown in tab. 2. Another notable component is ferric sulphate. Mounts of ferric sulphate were observed in the ash samples of the second-stage LTE. One part of the iron element may come from the coal, and the rest may be belonged to the metal wall of the second-stage LTE because of the severe corrosion by sulphuric acid, as shown in fig. 3.

Microscopic observation

It can be seen from fig. 3 that the fouling deposit covering evenly on the surface of the blade is about 10 mm thick and its hardness is close to the setting cement. As shown in the left of fig. 7, the micromorphology of the deposit sample mainly consists of irregular flocculent particles and spherical particles, and these particles are adhering tightly. Two areas and two spots in fig. 7 were selected to identify the difference in chemical composition. The mass

percentages of the elements detected are listed in tab. 4. There were approximately 27.2% and 26.9% of sulphur in ash deposits found in areas A and B, respectively. The result indicates that sulphate is widely distributed on the samples. Meanwhile, there were about 26.31% and 18.03% of silicon appearing in spots C and D, respectively. The high concentration of aluminium, calcium, potassium, and sodium were found in the samples, which means that the spherical particles may be the fly ash particles. Compared with the data in tab. 3, the content of the sulphur detected by EDS was larger, which indicated that the sulphate may cover the fly ash particles and result in higher concentration of sulphur on the surface of the samples. Therefore, the micromorphology of the induced fan blade indicates that the sulphate adhere firstly to the surface of particles and then form a sticky whole.

As shown in fig. 3, the deposits on the fined tubes of the second-stage LTE are loose and fragile. It is clear that the fouling deposits can be divided into three layers by colour. The inner layer close to the wall is reddish-brown because of the corrosion of the metal wall. Then the middle layer is grey, while the outer layer is pale yellow. This phenomenon indicates that the middle layer may be from fly ash particles in the flue gas, and the outer layer may be rich in sulphate. The right of fig. 7 presents the micromorphology of the sample collected at the finned tubes shown in the right of fig. 3. Different from the sample from the induced fan blade, the micromorphology of the samples from the second-stage LTE shows that the ash is consisted of lumpy particles with clear boundaries between adjacent clumps. One area and three spots were chosen to be analysed by EDS, and the high percentages of sulphur were found in all of the four sites. The result proves that the sulphate is the main substance of the fouling deposits. In the spot F, the content of iron was about 25.43% higher than others. Considering the severe corrosion shown in fig. 4, the iron in the samples may be partly due to the corrosion of metal wall of the finned tube. The content of the sulphur in all of the sites listed in tab. 4 is much higher than the total of the other elements. Combined with the XRD patterns in fig. 6, the concentration difference implies that ammonium alum and letovicite exist in the deposit samples.

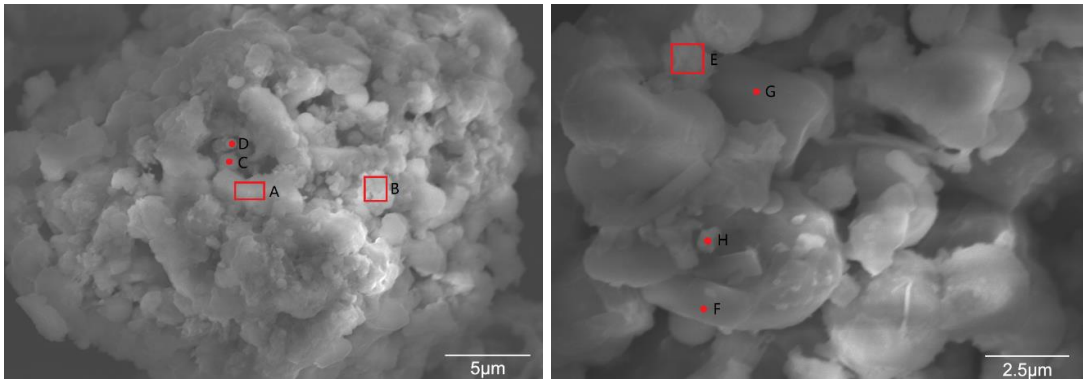

Figure 7. Micromorphologies of the fouling deposit samples (left) on the induced fan blade and (right) on the second-stage LTE

Fouling mechanism

According to the above results and analysis, the fouling mechanism of sulphate on the induced fan blade and the second-stage LTE can be summarized the four ways as shown in fig. 8. When SO_3 reacts with water vapour to form sulphuric acid droplets, some of the droplets

Table 4. EDS analyses of ash on the induced draft fan and the outlet of second-stage LTE

Elements [wt.%]	Sample on the induced draft fan				Sample on the outlet of second-stage LTE			
	Area A	Area B	Spot C	Spot D	Area E	Spot F	Spot G	Spot H
O	50.5	49.2	41.2	42.0	35.9	34.2	48.0	34.2
Mg	0.8	NT	0.6	0.6	1.2	NT	0.6	0.8
Al	5.8	7.6	9.3	10.0	9.2	3.5	4.9	4.2
Si	9.6	10.6	26.3	18.0	19.5	3.8	14.4	5.2
S	27.1	26.9	14.3	18.1	28.8	30.9	23.8	36.7
Ca	2.3	2.4	2.5	5.0	2.3	1.6	1.7	14.6
Fe	3.7	3.4	3.1	4.2	3.2	25.4	6.6	3.4
K	NT	NT	2.0	1.3	NT	NT	NT	1.0
Na	NT	NT	0.8	0.8	NT	0.6	NT	NT

Note: NT represents the element is not detected.

are deposited directly near the wall area where the temperature is lower. Then some of sulphuric acid is adsorbed by ash particles in the form of sulphuric acid vapour, or condensed directly on the surface of ash particles; eventually, all of them will be covered the surface of ash particles, promoting the agglomeration between ash particles, as well as the adhesion between the particles and the wall surfaces. There is also a part of sulphuric acid which absorbs ammonia in the flue gas to form sulphates such as ammonium hydrogen sulphate, ammonium sulphate and ammonium hydrogen hydroxide. The hyfroscopic sulphate has a certain viscosity, which further improves the adhesion ability of ash particles and wall surfaces. Finally, sulphuric acid, sulphate and ash particles adhere to the metal surface after colliding with it, and the fouling deposits are formed.

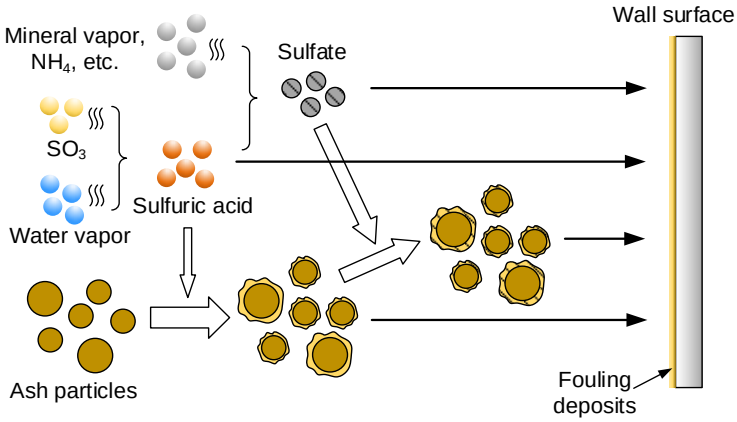

Figure 8. Fouling mechanism of sulphate on the blade and the wall surface

At the location of the induced fan, the complex flow field increases the probability of collision between the viscous particles and the metal surfaces. On the surface of the induced fan blade, with the increase of deposit thickness, the temperature of the inner deposition layer gradually drops below the melting point of the ammonium alum and the substance starts to solidify, so that the fouling deposit hardens into a hard cement-like ash. In addition,

the large temperature difference between the inlet and the outlet of the second-stage LTE is also an important factor causing serious fouling. On the wall surface of the heat exchanger, the ash particles are covered with less sulphate such as ammonium alum, and the viscosity of the deposit is relatively weak. Meanwhile, the cooling capacity of the second-stage LTE is strong, and the sulphuric acid droplets and sulphates are more likely to condense into solids on the wall surface, so the loose and fragile deposits are formed.

Conclusions

Severe fouling deposits were found on the induced fan blade and the second-stage LTE in a 1000MW coal-fired power plant with ultra-low emission. The ash samples were collected and analysed using XRD, XRF, SEM-EDS, and Element Analyser to reveal the main causes of severe fouling deposits. Firstly, it is found that the main components of the ash samples on the induced fan blade are tschermigite $(NH_4)Al(SO_4)_2 \cdot 12H_2O$, godovikovite $(NH_4)Al(SO_4)_2$, letovicite $(NH_4)_3H(SO_4)_2$, calcium sulphate $CaSO_4$, calcium sulphate dehyrate $CaSO_4 \cdot 2H_2O$, and quartz SiO_2. The main components of ash samples in the second-stage LTE are tschermigite $(NH_4)Al(SO_4)_2 \cdot 12H_2O$, ferric sulphate $Fe_2(SO_4)_3$, calcium sulphate $CaSO_4$, and quartz SiO_2. Then, it can be concluded that ammonium sulphate is the main component of the fouling deposits, which acts as an adhesive and make a contribution to the fouling deposits. Meanwhile, the continuous escape of high-concentration ammonia in the SCR system is also one of the important causes. Finally, it can be suggested that the temperature drop of the LTE should be designed based on the coal quality, ammonia slip quantity, ash concentration and so on. The LLT-ESP should be prevented from going beyond the state of the low temperature operation; otherwise, it will result in a large amount of sulphuric acid condensed on the low temperature zone of the downstream of LLT-ESP.

Acknowledgement

This work is supported by the National Natural Science Foundation of China (No. 51876162).

References

[1] Wang, G., *et al.*, Persistent Sulfate Formation from London Fog to Chinese Haze, *Proc. Natl. Acad. Sci. Unit. States. Am.*, *48* (2016), 113, pp. 13630-13635
[2] Fu, H., Chen, J., Formation, Features and Controlling Strategies of Severe Haze-Fog Pollutions in China, *Sci. Total Environ.*, *578* (2016), Feb., pp. 121-138
[3] Zhao, S. L., *et al*., Migration and Emission Characteristics of Trace Elements in a 660 MW Coal-Fired Power Plant of China, *Energ. Fuel*, *30* (2016), 7, pp. 5937-5944
[4] Andreas, B., *Enhancing ESP Efficiency for High Resistivity Fly Ash by Reducing the Flue Gas Temperature*, Springer-Heidelberg, Berlin, 2009
[5] Chen, T. M., *et al*., An Efficient Wet Electrostatic Precipitator for Removing Nanoparticles, Submicron and Micron-Sized Particles, *Sep. Purif. Technol.*, *136* (2014), 136, pp. 27-35
[6] Zhu, J., *et al*., Effects of High-Voltage Power Sources on Fine Particle Collection Efficiency with an Industrial Electrostatic Precipitator, *J Electrostat*, *70* (2012), 3, pp. 285-291
[7] Chen, Y., *et al*., Study on Ultra-Low Emission Reform Scheme of 1000 MW Coal Fired Unit, *Environmental Engineering*, *33* (2012), S1, pp. 1026-1029
[8] Zhao, Y. C., *et al*., Status of Ultra-Low Emission Technology in Coal-Fired Power Plant, *Journal of China Coal Society*, *40* (2015), 11, pp. 2629-2640
[9] Srivastava, R. K., *et al*., Nitrogen Oxides Emission Control Options for Coal-Fired Electric Utility Boilers, *Air Repair*, *55* (2005), 9, pp. 1367-1388
[10] Ma, Z. Z., *et al*., Characteristics of NO_x Emission from Chinese Coal-Fired Power Plants Equipped with New Technologies, *Atmospheric Environment*, *131* (2016), Apr., pp. 164-170

[11] Hans, J. H., *et al*., SCR Design Issues in Reduction of NO_x Emissions from Thermal Power Plants, Report, Frederikssund: Haldor Topsoe Inc., Lyngby, Denmark, 2007
[12] Shi, Y. J., *et al*., Formation and Decomposition of NH_4HSO_4 During Selective Catalytic Reduction of NO with NH_3 over V_2O_5-WO_3/TiO_2 Catalysts, *Fuel Process Technol.*, *150* (2016), Sept., pp. 141-147
[13] Menasha, J., *et al.*, Ammonium Bisulfate Formation Temperature in a Bench-Scale Single-Channel Air Preheater, *Fuel*, *90* (2011), 7, pp. 2445-2453
[14] Chothani, C., Ammonium Bisulfate (ABS) Measurement for SCR NO_x Control and Air Heater Protection, Breen Energy Solution, Carnegie, Penn., USA, 2008, Paper 51, pp. 1-13
[15] Sui, Z. F., *et al*., Fine Particulate Matter Emission and Size Distribution Characteristics in an Ultra-Low Emission Power Plant, *Fuel*, *185* (2016), Dec., pp. 863-871
[16] Grass, N., *et al*., Application of Different Types of High-Voltage Supplies on Industrial Electrostatic Precipitators, *IEEE Transactions on Industry Applications*, *40* (2004), 6, pp. 1513-1520
[17] Peng, W., *et al*., Kinetics Analysis on Mixing Calcination Process of Fly Ash and Ammonium Sulfate, *Chinese J Chem Eng*, *22* (2014), 9, pp. 1027-1032
[18] Huy, D. H., Development of Simultaneous Measurement Method of Gaseous Ammonia and Fine Particulate Ammonium and Study on Their Behaviors in Urban Atmosphere, Ph. D. thesis, Osaka Prefecture University, Osaka, Japan, 2016

Paper submitted: March 11, 2020
Paper revised: April 12, 2020
Paper accepted: April 15, 2020